

Four Flavor Finite Temperature Phase Transition with HYP Action: Where is the First Order Endpoint?

Anna Hasenfratz^y and Francesco Knechtli^z

Physics Department, University of Colorado,
Boulder, CO 80309 USA

Abstract

We study the finite temperature phase transition of four flavor staggered fermions with hypercubic fat link actions on $N_t = 4$ and $N_t = 6$ temporal lattices. Our fat links are constructed with hypercubic blocking (HYP) and therefore are very compact. We present a new algorithm for simulating fermions coupled to HYP fat links. The algorithm has a simple form based on the standard overrelaxation and heatbath updatings for the pure gauge action. We observe that as we increase the smoothness of the gauge fields by changing the parameters of the HYP blocking the very pronounced first order phase transition of the thin link action becomes weaker and moves to physically uninteresting values of the gauge coupling. With our smoothest HYP action we do not find any indication of a phase transition even at quark masses comparable to the physical light quark mass. We argue that the observed difference in the phase diagram is due to the improved flavor symmetry of the fat link actions.

PACS number: 11.15.Ha, 12.38.Gc, 12.38.Aw

^y e-mail: anna@eotvos.colorado.edu

^z e-mail: knechtli@pizero.colorado.edu

I. INTRODUCTION

Understanding the finite temperature phase structure of QCD has always been at the center of lattice studies. Recently all efforts have been focused on two and 2+1 flavor investigations [1], hardly any work looked at four flavor QCD [2, 3, 4, 5, 6, 7, 8]. This is not surprising, since early numerical results confirmed the theoretical expectations of the four flavor QCD phase diagram and computer resources were quickly directed towards the physically more interesting two and 2+1 flavor cases.

Based on universality Pisarski and Wilczek argued that QCD with $n_f = 3$ massless quark flavors has a first order chiral phase transition [9]. At finite quark mass the $n_f^2 - 1$ degenerate massive Goldstone bosons can destroy the phase transition. Above some critical mass value m_{max} one expects only a crossover. Numerical results using thin link staggered fermions confirmed the first order phase transition and determined the critical endpoint on $N_t = 4, 6$ and 8 lattices. Since the pure gauge $SU(3)$ theory has a first order deconfining phase transition, at very large quark masses one might again observe a first order transition but numerical simulations have not explored that region. It is only a small shadow on the otherwise satisfying picture that the numerically observed critical mass, m_{max} , does not scale as the temporal lattice size increases from four to six. This small “imperfection” can be explained by scaling violations at large lattice spacing [7].

Just because numerical simulations seemingly agree with theoretical expectations does not mean that we have the correct physical picture. The Pisarski-Wilczek argument is based on the $SU(n_f) \times SU(n_f)$ symmetry of the fermion action and the existence of $n_f^2 - 1$ degenerate Goldstone bosons in the chirally broken phase. Staggered fermions, on the other hand, break flavor symmetry. There is only a remnant $U(1)$ symmetry and a single true Goldstone boson in staggered simulations. The other, “would-be” Goldstone bosons are massive pseudoscalar particles even at vanishing quark mass. The full chiral symmetry is recovered only in the continuum limit. At the lattice spacing corresponding to $N_t = 4$ critical temperature the flavor symmetry violation of the thin link staggered action is substantial, the Pisarski-Wilczek scenario is not applicable.

Chiral symmetry breaking in QCD is closely related to the topological structure of the vacuum. Recently it was shown that the topological susceptibility measured on two- or four-flavor thin link staggered fermion configurations at lattice spacing $a \approx 0.17\text{fm}$ does not

follow the theoretically predicted chiral behavior at small quark masses [10]. Rather, the topological susceptibility appears to be consistent with the quenched value independently of the quark mass, implying that the thin link staggered fermions at that lattice spacing do not act like two or four degenerate flavors. The corresponding vacuum, at least regarding instantons, is closer to the quenched than to the dynamical vacuum. One has to reduce the lattice spacing to $a \approx 0.1 \text{ fm}$ to get acceptable, though still slightly high, values for the topological susceptibility. If instantons are responsible for chiral symmetry breaking, the chiral finite temperature phase transition should show similar *lattice artifacts*. The critical temperature of the chiral restoring phase transition is expected to be $T_c \approx 150 - 170 \text{ MeV}$ [8]. A lattice spacing $a \approx 0.17 \text{ fm}$ then corresponds to a critical system with temporal lattice extension $N_t = 1/(Ta) \approx 7 - 8$, a lattice spacing $a \approx 0.1 \text{ fm}$ corresponds to a system with $N_t \approx 12 - 14$. Therefore, if the indications from topology apply to the chiral phase transition, one has to use very large lattices, $N_t > 8$, to study the finite temperature phase transition with thin link staggered fermions.

There is no strong dependence on the number n_f of fermion flavors in the above argument, assuming that the critical temperature does not depend strongly on n_f . The two flavor case could show additional sensitivity to the topology of the vacuum. Pisarski and Wilczek argue that the $n_f = 2$ phase transition with massless quarks can be either first or second order, depending on the instanton density of the vacuum [9]. On the other hand the phase transition for $n_f \geq 3$ massless flavors is expected to remain first order independently of the instanton density. These considerations indicate that in order to reproduce the physical phase diagram on the lattice the instanton content of the vacuum should not be suppressed by lattice artifacts.

Flavor symmetry can be considerably improved by coupling the fermions to fat links [11, 12, 13]. Improved flavor symmetry leads to improved topology. The first results of Ref. [10] indicate that fat link actions can reproduce the quark mass dependence of the topological susceptibility even at lattice spacing $a \approx 0.17 \text{ fm}$. It is possible that even coarser lattices can be used with fat link fermions though it is unlikely that a much larger lattice spacing is allowed because instantons fall through the lattice when their radius is comparable to the lattice spacing, $r \approx a \approx 1$. Since the average instanton radius is $r \approx 0.3 \text{ fm}$, configurations with $a \approx 0.3 \text{ fm}$ will not have correct chiral behavior. Because of that dynamical lattices with temporal extension $N_t = 4$ are probably too coarse to reproduce the correct continuum

chiral behavior even with chiral fermions, $N_\tau = 6 - 8$ might be acceptable with chiral or almost chiral fermions.

In a recent publication we proposed an algorithm to simulate dynamical fat link actions [13]. In this paper we use a modified version of that method to study the phase diagram of four flavor staggered fermions on $N_\tau = 4$ and $N_\tau = 6$ temporal lattices. We use a new type of fat link action created with a hypercubic block (HYP) transformation [14]. The HYP blocking mixes gauge links within hypercubes attached to the original link only so that lattice artifacts due to extended smearing are minimized. The HYP fat links are so compact that the static potential is indistinguishable from the thin link one at distances $r=a-2$, yet flavor symmetry with staggered quarks is improved by about an order of magnitude. Our results for the finite temperature phase diagram with HYP staggered fermions deviate significantly from the thin link action predictions. At $N_\tau = 4$ and constant physical quark mass values the strongly first order phase transition observed with thin links weakens and moves deep into the strong coupling region as fattening is introduced. It appears that the $N_\tau = 4$ first order phase transition with thin link staggered fermions is more a lattice artifact than a physical phase transition. With our smoothest HYP action we do not see any sign of a first order phase transition even at quark masses comparable to the physical light quark mass, neither on $N_\tau = 4$ nor on $N_\tau = 6$ lattices. Because of the large lattice spacing at $N_\tau = 4$ even a chirally symmetric action might not be reliable but the $N_\tau = 6$ results should be closer to the continuum behavior. We believe that the observed difference between the HYP and thin link actions is due to the 15 near-degenerate Goldstone bosons of the fat link HYP action which destroy the first order transition, predicted at vanishing quark mass, even with very light quarks.

There are several groups doing calculations using dynamical fat link actions though with fat links that are less smooth than the HYP fat links [15, 16]. Unfortunately they did not publish results about the finite temperature phase transition with four flavors or on the topological susceptibility with either two or four flavors using fat link actions. We feel that the topological susceptibility is one of the best indicators to distinguish quenched and dynamical configurations and verify the effect of the sea quarks on the vacuum. Since Ref. [10] has only preliminary results using a different fat link action than considered here, we are presently investigating the topological susceptibility of the HYP action at different lattice spacings and quark masses. Early results show consistency with the theoretically predicted

chiral behavior at a lattice spacing $a = 0.17\text{fm}$ and at a quark mass corresponding to a Goldstone pion mass $m_\pi r_0 = 2.0$. Detailed results will be presented in a forthcoming publication [17].

This article is organized as follows. In Sect. 2 we present our new algorithm to simulate fat link actions. It is based on the standard overrelaxation and heatbath updatings for the pure gauge action. We describe the actions used in this study and the performance of the algorithm. In Sect. 3 we present our finite temperature results for four flavors of staggered fermions. We show how the phase diagram at $N_t = 4$ is changed by smoothing the gauge fields. With our smoothest HYP action we study the phase diagram when the quark mass is lowered and the spatial volume is increased. We also simulate the HYP action on finer lattices at $N_t = 6$. There is no sign of a first order phase transition even with very light quarks. In Sect. 4 we conclude with a summary.

II. SIMULATIONS

A. Algorithm

Dynamical simulations of fat link actions are difficult because the fermions couple to a complicated, extended, and, in case of projected fat links, non-linear combination of the gauge links. In [13] we considered fat links created by several levels of projected APE blocking. We introduced an auxiliary gauge field for each blocking level and coupled the fermions to the last level of auxiliary gauge fields.

In this article we present a new action that has no auxiliary gauge fields and can be simulated in a simpler way. Our new fat link action is

$$S = -\frac{1}{3} \sum_p \text{ReTr}(U_p) - \text{tr} \ln [M^{-1}(V)M(V)]; \quad (1)$$

where U_p is the plaquette product of the thin gauge links U_{ij} , M is the fermionic matrix and V_{ij} is the fat link that couples to the fermions. We denote by Tr the trace over $SU(3)$ color whereas tr means the trace over space-time indices i, j , directions μ, ν , spin and color. If the fat links are constructed in a deterministic way from the thin gauge fields, they are no longer dynamical variables and an ergodic update of the U fields will correctly simulate the system. Fat links can even be constructed by iterating the block transformation several times and

projecting back onto $SU(3)$ after each blocking step. The general algorithm to simulate the action of eq(1) is based on a two-step decomposition of the action. First, a subset of the thin links are updated with the standard microcanonical overrelaxation [18, 19] or Cabibbo-Marinari heatbath [20] algorithms for the pure gauge action $S_G(U) = -\frac{1}{3} \sum_p \text{ReTr}(U_p)$. Next, the deterministically constructed fat links are updated and this change is accepted with probability

$$P_{acc}(V^0; V) = \min \{1, \exp[-S_F(V^0) + S_F(V)]\}; \quad (2)$$

where V^0 denotes the new fat link configuration and $S_F(V) = -\text{tr} \ln [M^{\psi}(V)M(V)]$ is the fermionic action. The sequence of thin link updates must be carefully chosen to satisfy detailed balance with respect to the pure gauge action S_G . The proof that this algorithm satisfies detailed balance with respect to the full action $S = S_G + S_F$ follows closely the proof given in [21] for a similar two-step decomposition of the action.

In the practical implementation of the algorithm we choose the subset of thin links to be updated differently for the overrelaxation and for the heatbath steps. For the overrelaxation we reflect all the links within some finite block of the lattice. The location of the block is chosen randomly but its dimensions are fixed. We choose with probability 1/2 a given sequence of reflections within this block or with equal probability the reversed sequence. The sequence has to be reversed with respect to the direction and location of the thin links and with respect to the index of the $SU(2)$ subgroup used in the reflection step. For the heatbath we choose the subset of thin links randomly, i.e. we choose a random direction, a random parity, a set of random sites and a random sequence of $SU(2)$ subgroups. The probability of generating a given sequence of thin link updates or the reversed sequence is then the same, both for overrelaxation and heatbath. From this it follows that detailed balance with respect to the pure gauge action S_G is satisfied for both updatings. We chose to update a contiguous block of links with overrelaxation in order to propagate a change through (a portion of) the lattice. We observed that a random sequence of overrelaxed reflections is less efficient, especially for changing the topological charge of the configurations. This can be understood by thinking of instantons as extended objects. One has to change an entire region of the lattice to destroy or to create them.

The acceptance probability eq(2) contains the ratio of fermionic determinants $\det M^{\psi}(V^0)M(V^0) / \det M^{\psi}(V)M(V)$ which we evaluate by the same method as described in [13]. To make this article self-contained we summarize the steps in the following. First,

we remove the most ultraviolet part of the fermion matrix by decomposing it as

$$M(V) = M_r(V)A(V) \quad \text{with} \quad (3)$$

$$A(V) = \exp^h \left[-\frac{1}{4} D^4(V) + \frac{1}{2} D^2(V) \right]; \quad (4)$$

where D is the kinetic part of the fermion matrix and the parameters $\frac{1}{4}$ and $\frac{1}{2}$ are arbitrary but real. This way we achieve that an effective gauge action

$$S_{\text{eff}}(V) = -\frac{1}{2} \frac{1}{4} \text{Re tr} [D^4(V)] - \frac{1}{2} \frac{1}{2} \text{Re tr} [D^2(V)] \quad (5)$$

is removed from the determinant. The acceptance probability eq(2) can be approximated by the stochastic estimator

$$P_{\text{acc}}^0(V^0; V) = \frac{1}{n} \sum_{i=1}^n \exp \left[-S_{\text{eff}}(V) + S_{\text{eff}}(V^0) + \frac{1}{Y} M_r^Y(V^0) M_r(V^0) - M_r^Y(V) M_r(V) \right]; \quad (6)$$

where the vector Y is generated according to the probability distribution

$$P(Y) \propto \exp \left[-\frac{1}{Y} M_r^Y(V^0) M_r(V^0) \right]; \quad (7)$$

The parameters $\frac{1}{2}$ and $\frac{1}{4}$ can be optimized to maximize the acceptance rate. We keep the same choice $\frac{1}{2} = 0.18$ and $\frac{1}{4} = 0.006$ as in [13].

B. Actions

In this study of the QCD thermodynamics we use four flavors of staggered fermions and compare results obtained with three different fermionic actions. Besides the standard action with thin link gauge connections, we simulate two fat link actions of the form eq(1): the APE1 action and the HYP1 action. The simple form of the action and of the algorithm based on overrelaxation and heatbath updatings with respect to the gauge action allows us to simulate fat link action with any fattening procedure. No further improvement of the gauge and fermionic actions is used here.

In the APE1 action the fat links are constructed using only one level of APE smearing with APE parameter $\alpha = 0.7$ [22]. The fat link is defined as

$$V_{ij} = \text{Proj}_{\mathcal{B} \cup \{3\}} \left[(1 - \frac{\alpha}{6}) U_{ij} + \frac{\alpha}{6} \sum_{\mu \in \mathcal{B}} U_{ij} U_{i+\mu} U_{i+\mu}^Y \right]; \quad (8)$$

Action/ α_2 ()	Thin	APE1	HYP1
$i\bar{j}5$	0.594(25)	0.212(22)	0.086(14)
$i\bar{j}j$	0.72(6)	0.35(5)	0.150(24)

TABLE I: The parameter α_2 measuring flavor symmetry violations as computed in the quenched approximation at $\beta = 5.7$ for the different quark actions that we use in this study.

where the projection onto $SU(3)$ is deterministic. In the HYP1 action the fat links are constructed using one level of hypercubic (HYP) blocking and we refer to Ref. [14] for the precise definition and the parameter choice of the HYP fattening. The HYP fat links mix thin links within the hypercubes attached to the original link only. The artifacts due to extended smearing, e.g. in the static potential at short distances, are minimized with the HYP blocking. At the same time the improvement of chiral or flavor symmetry is substantial. In [14] it has also been demonstrated that one level of HYP blocking remains effective as the lattice spacing is decreased. Finally, the APE smearing can be considered as a particular choice of the parameters of the HYP smearing.

To compare the flavor symmetry violations of the standard, APE1 and HYP1 actions we calculated the quenched pion spectrum on an ensemble of $\beta = 5.7$, $8^3 \times 24$ pure gauge configurations with lattice spacing $a' = 0.17$ fm. As we demonstrated in [13] the quenched result is a good indication of the dynamical flavor symmetry violations. We use the parameter [11]

$$\alpha_2 = \frac{m^2 - m_G^2}{m^2 + m_G^2} \quad (9)$$

at $m = m_\pi = 0.55$ to quantify the difference between the mass of the true Goldstone pion m_G and the mass of the pseudoscalar particles (or pions) m_π . The results are summarized in table I. We compute the parameter α_2 for the two lightest non-Goldstone pions, $i\bar{j}5$ with flavor structure δ_{i5} , and $i\bar{j}j$ with flavor structure δ_{ij} . For a flavor symmetric action $\alpha_2 = 0$. The flavor symmetry violation of the thin link action is reduced by a factor 3 with the APE1 action and by a factor 6 with the HYP1 action at this lattice spacing.

In figure 1 we plot the square of the Goldstone pion mass m_G in units of the Sommer scale r_0 [24] as function of the bare quark mass am_q . In addition to the three valence actions used in this study we plot the data for the APE3 action (3 levels of APE smearing with $\beta = 0.7$ and projection parameter $\beta = 500$) of Ref. [13]. The data for the three lowest quark masses with thin link action come from Ref. [23] and are obtained on $\beta = 5.7$; $16^3 \times 32$

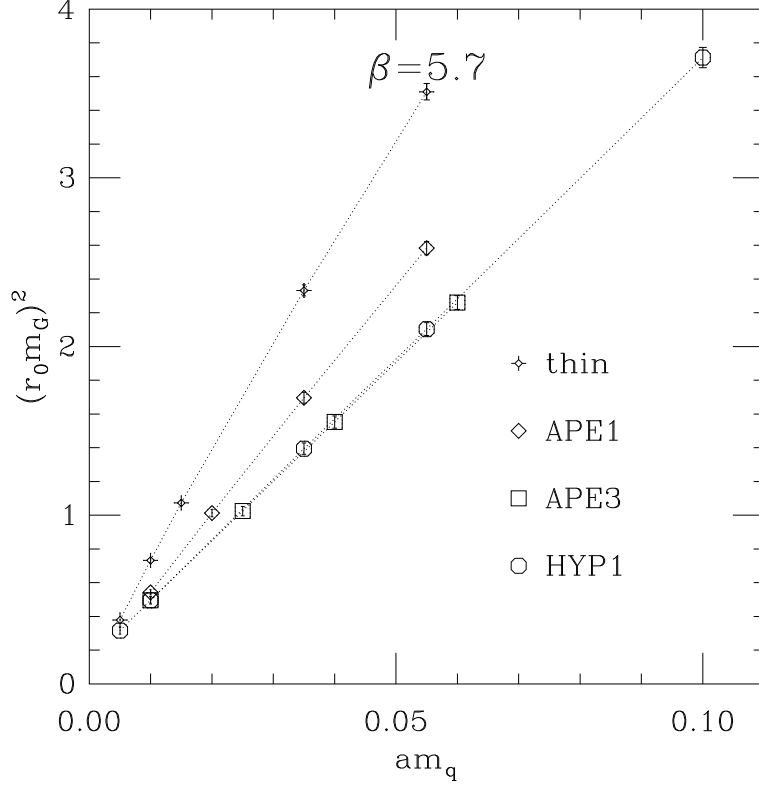


FIG. 1: The mass renormalization in the quenched approximation at $\beta = 5.7$ for different quark actions. The APE3 action is the fat link action of Ref. [13]. The three lowest quark mass values with thin link action are from Ref. [23].

lattices. The mass renormalization after one level of HYP blocking is the same as after 3 levels of APE blocking. We will use these quenched results to approximately match the physical quark masses between dynamical simulations of four flavors of HYP and thin link staggered fermions.

C. Performance

We would like to compare the performance of the algorithm described in section II A for the simulation of the HYP1 action with the standard HMC algorithm for the thin link action. We would like to emphasize that the implementation of the algorithm for the HYP1 action is very simple and can be easily parallelized. We also optimized our parallelized code reducing considerably the simulation time cost.

On $8^3 \times 24$ lattices we simulated the HYP1 action with gauge coupling $\beta = 5.2$ and

quark mass $am_q = 0.1$. An approximate matching of the lattice spacing and the physical quark mass can be achieved by simulating the thin link action with parameters $\beta = 5.2$ and $am_q = 0.06$. In an attempt to make a reliable comparison of the time costs, we estimated the autocorrelation times for simple observables like the plaquette and the chiral condensate $\langle \bar{\psi}\psi \rangle$. We found that measurements with thin link action separated by one HMC trajectory of unit time length have comparable autocorrelations as measurements with HYP1 action separated by 160 overrelaxation steps and 80 heatbath steps. Each overrelaxation step updates a block of 128 links, each heatbath step updates 200 links with an acceptance of about 20% for both updatings. In these physical time units the simulation of the HYP1 action is a factor of 7 more expensive than the thin link action.

Interestingly neither the heatbath nor the overrelaxation algorithm loses efficiency as the quark mass is lowered. With a combination of the two updates one can easily simulate systems at very small quark masses that would be impractical if not impossible to simulate with standard fermionic algorithms. We simulated on $8^3 \times 24$ lattices the HYP1 action with parameters $\beta = 5.2$, $am_q = 0.04$ and the thin link action with parameters $\beta = 5.2$, $am_q = 0.024$, with approximately matched physical quark masses. The time costs are now only a factor 3 higher for the HYP1 action as compared to the thin link action, due to the considerable increase of conjugate gradient steps needed in the inversion of the fermion matrix with thin links.

At a fixed lattice spacing the necessary number of overrelaxation and heatbath updating steps between independent configurations scales with the volume. Since each updating requires the evaluation of the fermionic action, this gives a volume square dependence for the cost of the algorithm. On the other hand the number of links that can be updated with the overrelaxation or heatbath algorithms scales with the lattice spacing, the necessary number of updating steps for a fixed physical volume is independent of the lattice spacing. We simulated the HYP1 action on temporal lattices with $N_t = 4$ and $N_t = 6$ time extensions. The change in lattice spacing corresponds to about a factor of 5 change in lattice volumes. At present we cannot match the physical scales between the $N_t = 4$ and $N_t = 6$ simulations. Nevertheless, comparing temperature regions where similar changes in the observables occur (e.g. the region where the chiral condensate starts increasing as the temperature is lowered) we notice that we can update about 5 times as many links on the $N_t = 6$ lattices than on the $N_t = 4$ lattices. This indicates that the physical volume of the updated region remains

constant as the continuum limit is approached.

III. FINITE TEMPERATURE RESULTS

In this finite temperature study we performed simulations at $N_t = 4$ on $8^3 \times 4$, $10^3 \times 4$ and $16^3 \times 4$ lattices and at $N_t = 6$ on $16^3 \times 6$ lattices. At $N_t = 4$ we considered both the APE1 and HYP1 actions and we will compare our results to thin link simulations. We used the data from quenched spectroscopy simulations shown in figure 1 to match approximately the quark masses of the different actions. The bare mass values used in our simulations are listed in table II. At the lowest quark mass value we simulated only the HYP1 action as it became computationally very demanding to simulate both the thin and APE1 actions. At $N_t = 6$ we simulated only the HYP1 action with a mass that corresponds to the lowest mass at $N_t = 4$. To get a feeling for the physical value of the masses, assuming a critical temperature $T_c \approx 150 - 170 \text{ MeV}$ for four flavor QCD [8] and using $Z = 1$ for the mass renormalization factor we estimate that the lowest quark mass simulations corresponds to $m_q \approx 6 - 7 \text{ MeV}$. Even though this estimate can easily have a factor of two to four error, this value is still very close to the physical light mass values.

The observables that we measure in our simulations are the average Polyakov loop

$$L = \frac{1}{N_s^3} \sum_{\mathbf{n}} \text{Tr} \prod_{t=0}^{N_t-1} U_{(\mathbf{n},t);0} \quad (10)$$

the susceptibility $\chi_L = N_s^3 \langle \bar{\psi} \psi \rangle^2 - \langle \bar{\psi} \psi \rangle^2$ and the chiral condensate

$$\bar{\psi} \psi = \frac{1}{N_s^3 N_t} \text{tr} M^{-1}(\mathbf{V}) = \frac{1}{10 N_s^3 N_t} \sum_{i=1}^4 \mathbf{R}_i^T M^{-1}(\mathbf{V}) \mathbf{R}_i \quad (11)$$

which we evaluate using 10 Gaussian random vectors \mathbf{R}_i per configuration.

A. Phase structure and flavor symmetry

Let us look first at the largest mass set, Set 1 in table II. Figures 2, 3 and 4 show the real part of the Polyakov line and $\langle \bar{\psi} \psi \rangle$ for the three actions on $8^3 \times 4$ lattices. The thin link action shows a pronounced discontinuity at $\beta \approx 5.1$. The jump in the Polyakov line is about 0.4, in $\langle \bar{\psi} \psi \rangle$ about 0.2. The APE1 action also gives indication of a first order phase transition at $\beta \approx 4.85$ but the discontinuity of the Polyakov line is only about 0.2, of

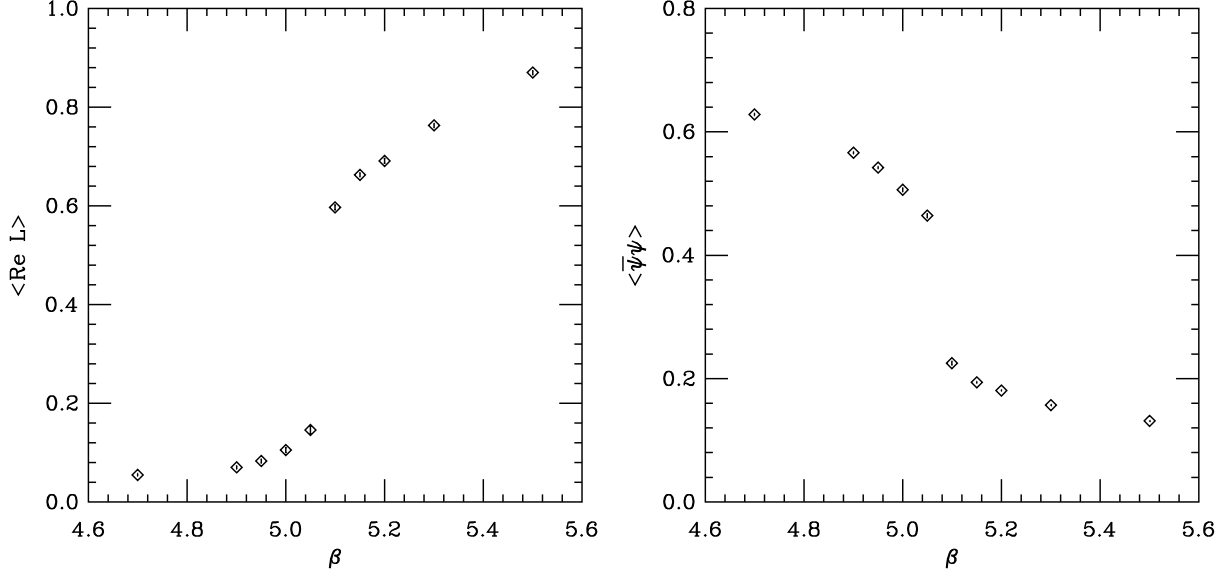


FIG. 2: Thin link action simulated on $8^3 \times 4$ lattices at quark mass $am_q = 0.06$ (Set 1 in table II). The real part of the Polyakov line and the chiral condensate $\langle \bar{\psi} \psi \rangle$ are plotted as a function of β .

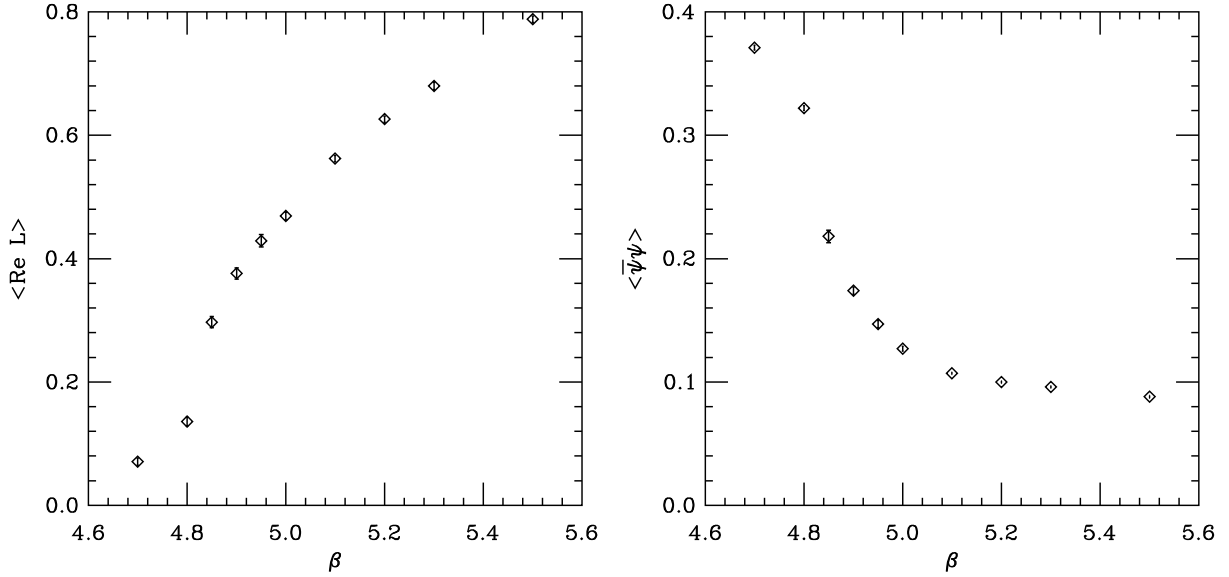


FIG. 3: APE1 action simulated on $8^3 \times 4$ lattices at quark mass $am_q = 0.08$ (Set 1 in table II). The real part of the Polyakov line and the chiral condensate $\langle \bar{\psi} \psi \rangle$ are plotted as a function of β .

Action/Set	Thin	APE1	HYP1	N_s
Set 1 ($N_\tau = 4$)	0.06	0.08	0.1	8
Set 2 ($N_\tau = 4$)	0.024	(0.032)	0.04	8, 10
Set 3 ($N_\tau = 4$)	(0.006)	(0.008)	0.01	8, 10, 16
Set 3 ($N_\tau = 6$)	(0.004)	(0.0053)	0.0067	16

TABLE II: The bare quark mass values am_q for the different actions that correspond to approximately the same physical mass. An entry in parenthesis indicates that we did not simulate that action in the data set. In the last column we list the spatial extension N_s of the lattices in our simulations.

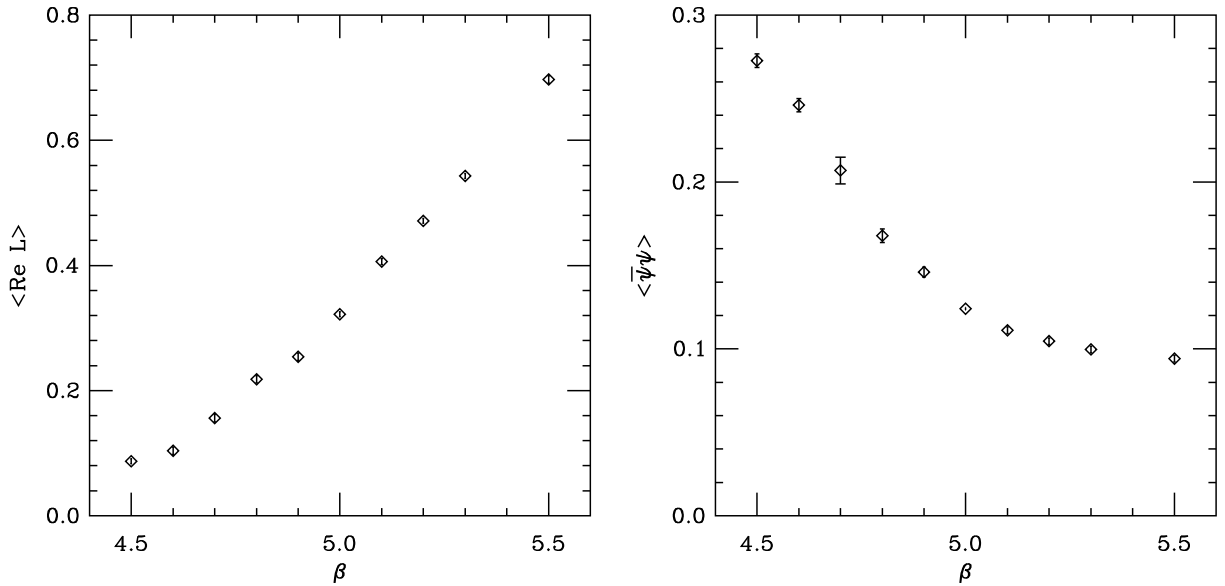


FIG. 4: HYP1 action simulated on $8^3 \times 4$ lattices at quark mass $am_q = 0.1$ (Set 1 in table II). The real part of the Polyakov line and the chiral condensate $\langle \bar{\psi} \psi \rangle$ are plotted as a function of β .

$\langle \bar{\psi} \psi \rangle$ about 0.1. Also, the discontinuity is at a lower β value with respect to the thin link action. Although we do not have a scale determination for the APE1 action, it is unlikely that the physical value of the phase transition temperature is unchanged. As figure 4 shows the discontinuity completely disappears with the HYP1 action. Both the deconfinement and chiral order parameters change smoothly from the low to the high temperature phase. Moreover the susceptibility χ_L of the Polyakov line does not show a peak as a function of the coupling β .

Action	β	am_q	r_0/a	a^{P}/a	a [fm]	m_π/m_G	m_ρ/m_π
HYP1	5.0	0.1	-	0.51(3)	0.23(2)	0.144(6)	0.66(2)
HYP1	5.2	0.1	2.94(3)	0.373(11)	0.17	0.057(6)	0.719(8)
thin	5.2	0.06	2.85(2)	0.40(1)	0.18	0.63(3)	0.56(2)

TABLE III: Physical scale and flavor symmetry violation of the dynamical HYP1 action. For comparison we list the corresponding values for the thin link action whose bare parameters are chosen to approximately match the physical scale and Goldstone pion mass of the $\beta = 5.2$, $am_q = 0.1$ HYP1 simulations.

The observation that the phase transition weakens as the gauge connections between fermions become smoother and eventually disappears for our smoothest HYP1 action is a strong indication that the phase transition of the thin link action is a lattice artifact. To support this further we determined the physical scale of the HYP1 action at two coupling values, $\beta = 5.0$ and $\beta = 5.2$, with mass $am_q = 0.1$ on $8^3 \times 24$ lattices. On the same configurations we also measured the meson spectrum. Our results are summarized in table III where we list the values for the Sommer scale r_0/a , the string tension a^{P}/a , the relative mass splitting m_π/m_G between the lightest non-Goldstone pion π_{15} and the Goldstone pion G and the pion to rho mass ratio. At $\beta = 5.0$ the violations of rotational symmetry in the static potential are substantial and we were not able to determine reliably r_0/a since it is too small. We could obtain a value for the string tension from which we get the lattice spacing quoted in table III. At $\beta = 5.2$ both quantities r_0/a and a^{P}/a give a consistent value for the lattice spacing. The point we would like to make is that, even if the HYP1 action would show some discontinuity below our lowest $\beta = 4.5$ value of figure 4, this would happen in a region where the lattice spacing is about 1 fm or larger, therefore it would be physically irrelevant.

Again, we see that the flavor symmetry restoration predicted by quenched simulations agrees with the dynamical results. The quenched study of Ref. [14] predicted, at a lattice spacing $a' = 0.17$ fm, a mass splitting $m_\pi/m_G = 0.049(8)$ with the HYP1 valence action at $am_q = 0.1$. As table III shows the dynamical simulations confirm this result. Flavor symmetry with the HYP1 action is an order of magnitude better than with the thin link action, as can be seen by comparing the results obtained with the thin link action at approximately matched

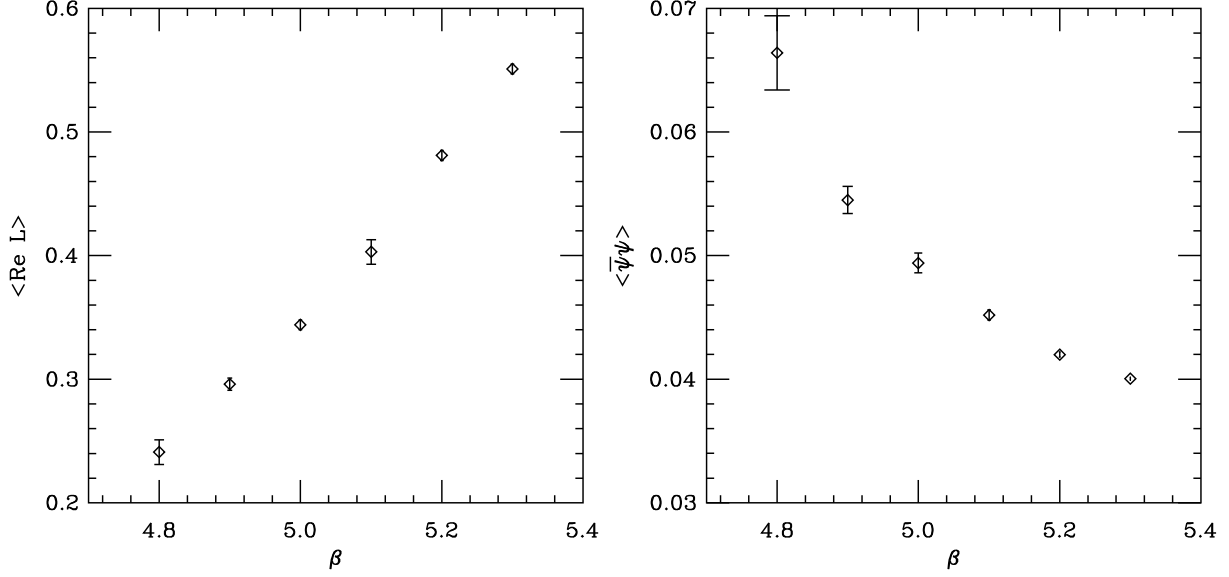


FIG. 5: HYP1 action simulated on $8^3 \times 4$ lattices at quark mass $am_q = 0.04$ (Set 2 in table II). The real part of the Polyakov line and the chiral condensate $\langle \bar{\psi} \psi \rangle$ are plotted as a function of β .

lattice spacing and Goldstone pion mass.

B. The phase diagram with the HYP action

The HYP1 action shows only a crossover with $am_q = 0.1$ quark mass. This might not be that surprising if we look at the endpoints of the first order phase transition lines for the thin link action quoted in [7]. At $N_t = 4$, $am_{max} \approx 0.073$ while at $N_t = 6$, $am_{max} \approx 0.021$, showing a substantial scale breaking. The physical mass of Set 1 is lower than m_{max} at $N_t = 4$ but larger than m_{max} one would predict from the $N_t = 6$ simulations assuming scaling.

In this section we consider the HYP1 action at smaller quark masses to see if we can find a first order phase transition. The quark mass of Set 2 is, in physical units, below the observed endpoint m_{max} of the $N_t = 6$ thin link transition. Numerical results for the thin link action at $am_q = 0.024$ on $8^3 \times 4$ lattices show a strong first order phase transition. Yet the results with the HYP1 action on $8^3 \times 4$ lattices plotted in figure 5 show only a very broad crossover.

Looking for the endpoint of the first order phase transition we simulated the HYP1 action

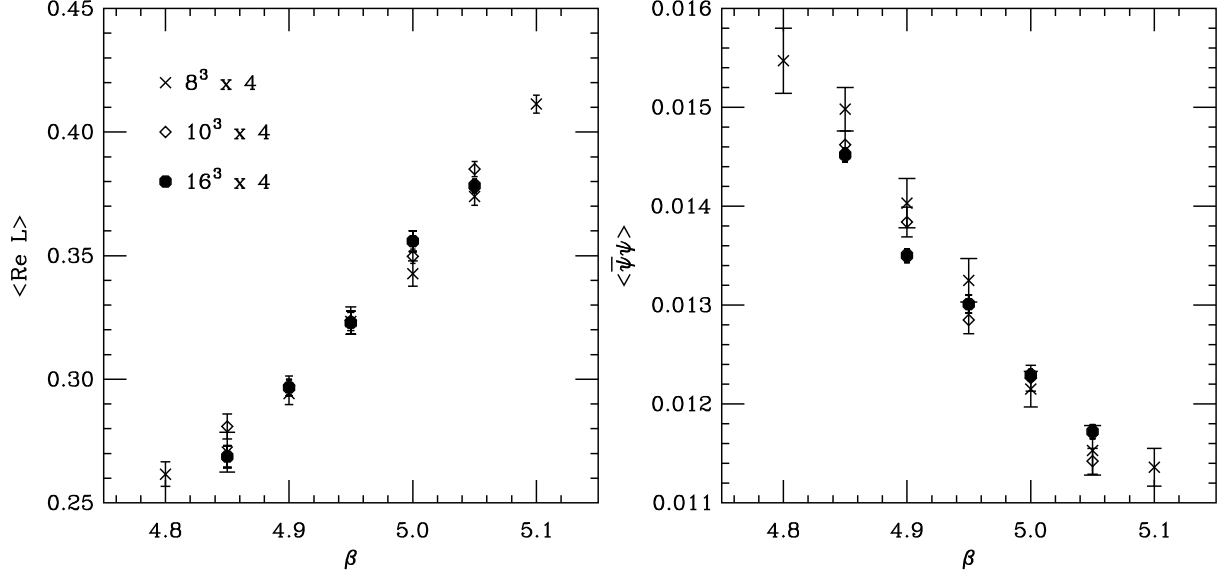


FIG. 6: HYP1 action simulated on $8^3 \times 4$ (crosses), $10^3 \times 4$ (diamonds) and $16^3 \times 4$ (octagons) lattices at quark mass $am_q = 0.01$ (Set 3 in table II). The real part of the Polyakov line and the chiral condensate $\langle \bar{\psi}\psi \rangle$ are plotted as a function of β .

at the even lower quark mass of Set 3, $am_q = 0.01$. At this low value of the quark mass finite volume effects might play a role. For example the first order phase transition observed with the thin link action at $N_t = 6$ on $16^3 \times 6$ lattices at a quark mass $am_q = 0.01$ in Ref. [6] washes away if we repeat the simulations on $8^3 \times 6$ lattices. To make sure that our results are not due to finite size effects we simulated the HYP1 action at quark mass $am_q = 0.01$ on $8^3 \times 4$, $10^3 \times 4$ and $16^3 \times 4$ lattices. The results are shown in figure 6. There is no sign of significant deviations as the spatial volume is increased by a factor of eight and the phase diagram shows a very broad crossover. We conclude that there is no first order phase transition at $N_t = 4$ for quark masses down to approximately the physical light quark mass.

In order to verify and understand the Pisarski-Wilczek scenario it would be important to locate the endpoint of the first order phase transition line. This, however, should not be done on $N_t = 4$ lattices. As we pointed out in the introduction, simulations at $N_t = 4$ might be questionable even with chirally symmetric actions because the lattice spacing is too large to support the correct topological structure of the vacuum. Furthermore, decreasing the quark mass while staying at $N_t = 4$ makes flavor symmetry violations larger even with the HYP1 action. We believe that the disappearance of the first order phase transition is due

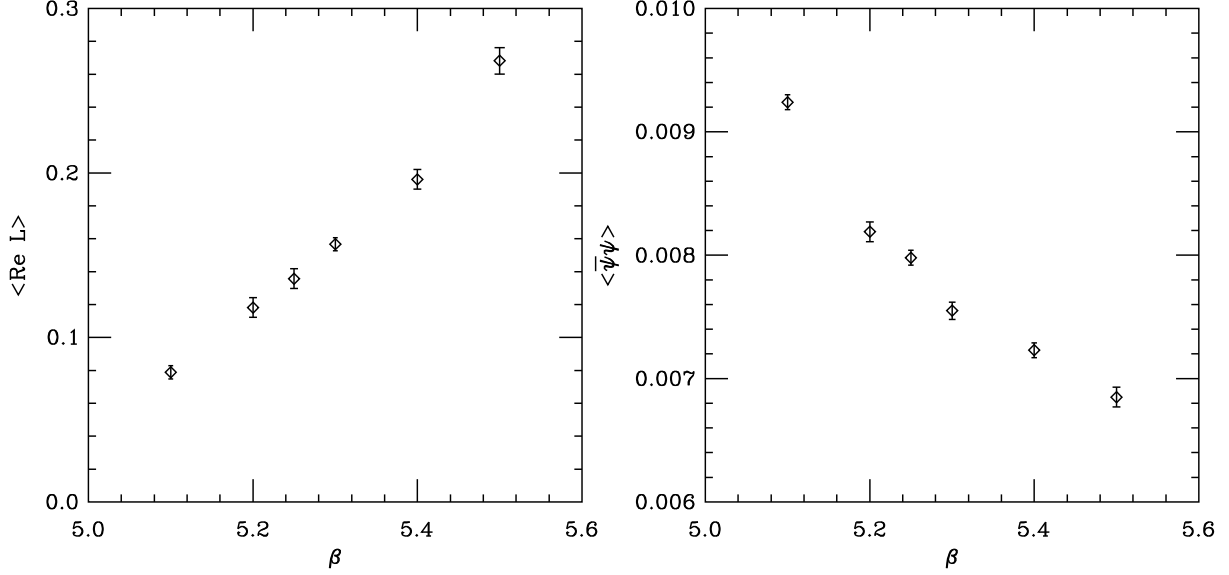


FIG. 7: HYP1 action simulated on $16^3 \times 6$ lattices at quark mass $am_q = 0.0067$ (Set 3 in table II). The real part of the Polyakov line and the chiral condensate $\langle \bar{\psi} \psi \rangle$ are plotted as a function of β .

to the improved flavor symmetry of the HYP1 action. These considerations indicate that physical results concerning the phase transition with light quarks can be obtained with the HYP1 action on $N_t = 6$ temporal lattices.

In figure 7 we show the results for $N_t = 6$ thermodynamics with HYP1 action on $16^3 \times 6$ lattices at a quark mass $am_q = 0.0067$. This mass matches approximately the lightest quark mass of Set 3 at $N_t = 4$. The critical region, which we identify as the region where $\langle \bar{\psi} \psi \rangle$ starts increasing and where the autocorrelation times are the largest, moves to higher values than at $N_t = 4$. Again, there is no sign of a first order phase transition, the Polyakov line and the chiral condensate are smooth, indicating a crossover as observed at $N_t = 4$. The Polyakov line susceptibility χ_L does not show any peak and its values agree with the ones obtained on the $N_t = 4$ lattices.

IV. SUMMARY

In this paper we studied the finite temperature phase diagram of four flavor fat link staggered fermion actions on lattices with $N_t = 4$ and $N_t = 6$ temporal extents. We used a new smearing, the hypercubic blocking (HYP), for the fat links. Hypercubic blocking mixes the gauge links only within hypercubes attached to the original link minimizing thereby the

lattice artifacts arising from extended smearing. The action with one level of hypercubic blocking (HYP1) considerably reduces the flavor symmetry breaking of the standard thin link action but does not change the local properties of the gauge fields beyond distances $r=a-2$. We presented a new algorithm for simulating the HYP1 action. This algorithm is very simple because it is based on the overrelaxation and heatbath algorithms for the pure gauge action. It is efficient as the quark mass or the lattice spacing are lowered allowing simulations which would be impractical with thin link action.

We found that improved flavor symmetry, presumably the presence of 15 near-degenerate Goldstone bosons, changes the finite temperature phase diagram of four flavor QCD. Our simulations with the HYP1 action do not show any sign of a first order phase transition even at physical quark masses of a few MeV, in contradiction with thin link action results.

Our algorithm to simulate the HYP1 action can be generalized to arbitrary number of flavors by using a polynomial approximation for the fermionic action.

V. ACKNOWLEDGEMENTS

We are indebted to M. Hasenbusch for discussions that lead to the new algorithm presented here. We benefited from many discussions with Prof. T. DeGrand during the course of this work. The simulations were performed in scalar and parallel mode on the beowulf cluster of the high energy theory group and on the linux farm of the high energy experimental group at University of Colorado. We would like to thank the system administrator, D. Johnson, for his precious technical support. This work was supported by the U. S. Department of Energy. Finally we thank the MILC collaboration for the use of their computer code.

-
- [1] S. Ejiri, Nucl. Phys. Proc. Suppl. **94**, 19 (2001), hep-lat/0011006.
 - [2] S. Gottlieb, W. Liu, D. Toussaint, R. L. Renken, and R. L. Sugar, Phys. Rev. **D35**, 3972 (1987).
 - [3] S. Gottlieb, W. Liu, R. L. Renken, R. L. Sugar, and D. Toussaint, Phys. Rev. **D40**, 2389 (1989).
 - [4] R. V. Gagai et al. (MT(c)), Phys. Lett. **B232**, 491 (1989).

- [5] R. V. Gavai et al. (MT(c)), Phys. Lett. **B241**, 567 (1990).
- [6] F. R. Brown et al., Phys. Lett. **B251**, 181 (1990).
- [7] S. Gottlieb, Nucl. Phys. Proc. Suppl. **20**, 247 (1991).
- [8] J. Engels et al., Phys. Lett. **B396**, 210 (1997), hep-lat/9612018.
- [9] R. D. Pisarski and F. Wilczek, Phys. Rev. **D29**, 338 (1984).
- [10] A. Hasenfratz (2001), hep-lat/0104015.
- [11] K. Orginos and D. Toussaint (MILC), Phys. Rev. **D59**, 014501 (1999), hep-lat/9805009.
- [12] K. Orginos, D. Toussaint, and R. L. Sugar (MILC), Phys. Rev. **D60**, 054503 (1999), hep-lat/9903032.
- [13] F. Knechtli and A. Hasenfratz, Phys. Rev. **D63**, 114502 (2001), hep-lat/0012022.
- [14] A. Hasenfratz and F. Knechtli (2001), hep-lat/0103029, accepted for publication in Phys. Rev. D.
- [15] F. Karsch, E. Laermann, and A. Peikert, Phys. Lett. **B478**, 447 (2000), hep-lat/0002003.
- [16] C. Bernard et al. (2001), hep-lat/0104002.
- [17] A. Hasenfratz and F. Knechtli (2001), in preparation.
- [18] S. L. Adler, Phys. Rev. **D23**, 2901 (1981).
- [19] R. Petronzio and E. Vicari, Phys. Lett. **B245**, 581 (1990).
- [20] N. Cabibbo and E. Marinari, Phys. Lett. **B119**, 387 (1982).
- [21] M. Hasenbusch, Phys. Rev. **D59**, 054505 (1999), hep-lat/9807031.
- [22] M. Albanese et al. (APE), Phys. Lett. **B192**, 163 (1987).
- [23] R. Gupta, G. Guralnik, G. W. Kilcup, and S. R. Sharpe, Phys. Rev. **D43**, 2003 (1991).
- [24] R. Sommer, Nucl. Phys. **B411**, 839 (1994), hep-lat/9310022.